Chemistry–A European Journal

Research Article
doi.org/10.1002/chem.202104552

Chemistry Europe
European Chemical
Societies Publishing

www.chemeurj.org

Novel Thienyl DPP derivatives Functionalized with Terminal Electron-Acceptor Groups: Synthesis, Optical Properties and OFET Performance

Sandra Fusco,[a] Mario Barra,[b] Lorenzo Gontrani,[c, f] Matteo Bonomo,[c, d] Federico Chianese,[b, e] Simone Galliano,[d] Roberto Centore,[a] Antonio Cassinese,[b, e] Marilena Carbone,[f] and Antonio Carella*[a]

Abstract: Three novel diketopyrrolopyrrole (DPP) based small molecules have been synthesized and characterized in terms of their chemical-physical, electrochemical and electrical properties. All the molecules consist of a central DPP electron acceptor core symmetrically functionalized with donor bi-thienyl moieties and flanked in the terminal positions by three different auxiliary electron-acceptor groups. This kind of molecular structure, characterized by an alternation of electron acceptor and donor groups, was purposely designed to provide a significant absorption at the longer wavelengths of the visible spectrum: when analysed as thin films, in fact, the dyes absorb well over 800 nm and exhibit a narrow optical bandgap down to 1.28 eV. A detailed DFT analysis provides useful information on the electronic structure of the dyes and on the features of the main optical transitions. Organic field-effect transistors (OFETs) have been fabricated by depositing the DPP dyes as active layers from solution: the different end-functionalization of the dyes had an effect on the charge-transport properties with two of the dyes acting as n-type semiconductors (electron mobility up to $4.4 \cdot 10^{-2}$ cm^2/V·s) and the third one as a p-type semi-conductor (hole mobility up to $2.3 \cdot 10^{-3}$ cm^2/V·s). Interest-ingly, well-balanced ambipolar transistors were achieved by blending the most performant n-type and p-type dyes with hole and electron mobility in the order of 10^{-3} cm^2/V·s

[a] Dr. S. Fusco, Prof. R. Centore, Prof. A. Carella
Dipartimento di Scienze Chimiche
Università degli Studi di Napoli 'Federico II', Complesso Universitario Monte Sant'Angelo
Via Cintia 21, 80126 Napoli (Italy)
E-mail: antonio.carella@unina.it

[b] Dr. M. Barra, Dr. F. Chianese, Prof. A. Cassinese
Dipartimento di Fisica "Ettore Pancini"
CNR-SPIN
P.le Tecchio, 80, 80125 Napoli (Italy)

[c] Dr. L. Gontrani, Dr. M. Bonomo
Dipartimento di Chimica
Università di Roma "La Sapienza"
Piazzale Aldo Moro 5, 00185 Roma (Italy)

[d] Dr. M. Bonomo, Dr. S. Galliano
Department of Chemistry and NIS Interdepartmental Centre
University of Torino
Via Pietro Giuria 7, 10125 Torino (Italy)

[e] Dr. F. Chianese, Prof. A. Cassinese
Dipartimento di Fisica "Ettore Pancini"
Università degli Studi di Napoli 'Federico II'
P.le Tecchio, 80, 80125 Napoli (Italy)

[f] Dr. L. Gontrani, Prof. M. Carbone
Dipartimento di Scienze e Tecnologie Chimiche
Università di Roma "Tor Vergata"
Via della ricerca scientifica 1, 00133 Roma (Italy)

Introduction

Diketopyrrolopyrrole (DPP) derivatives represent a class of molecular systems that have been widely investigated and employed in several applications of relevant technological appeal.[1–7] The DPP core structure was synthesized for the first time in the early 1970s.[8] Due to some outstanding properties such as beautiful and brilliant colour (ranging from orange to bluish red), high thermal stability and excellent photophysical properties, DPP derivatives are nowadays among the most important high-performance pigments, used in the fields of inks and paints, automotive industry, plastics and fibers.[9] In addition, the synthetic versatility in DPP chemistry has allowed the preparation of a large variety of derivatives being now applied in less conventional fields. First, by functionalizing the lactamic nitrogen of the DPP core, soluble derivatives can be achieved; then, different flanking groups can be introduced in 3,6-positions and a further extension of the conjugated molecular backbone can be obtained by means of C—C cross coupling reactions with different molecular fragments in the preparation of polymers or small molecules. The highly planar nature of the bi-lactamic fused bicycle constituting the DPP core, favours π-π interactions and, hence, positively affects charge transport properties. For this reason, DPP soluble derivatives have found a primary application in the realm of organic electronics: DPP small molecules or polymers have been used as donor materials[10–12] or, more recently, as non-fullerene acceptors (NFA) in bulk heterojunction organic solar

Chem. Eur. J. 2022, 28, e202104552 (1 of 12)

© 2022 The Authors. Chemistry - A European Journal published by Wiley-VCH GmbH

Chemistry–A European Journal

Research Article
doi.org/10.1002/chem.202104552

Chemistry Europe
European Chemical
Societies Publishing

cells.[4,13] Moreover, by combining DPP units with different molecular blocks (electron rich or poor), it is possible to obtain new systems with a tailored tuning of frontier molecular orbitals (highest occupied molecular orbital, HOMO, and lowest unoccupied molecular orbitals, LUMO) energies: by this modulation it has been possible to achieve the optimization of hole and electron mobility in p-type[14–18] and n-type materials,[19,20] respectively, for organic field-effect transistors (OFET). Several examples of ambipolar DPP derivatives have been also reported.[21–24] The synthetic versatility in DPP chemistry allowed the preparation of several near infrared (NIR) absorbing DPP containing materials: NIR absorbing materials have been gaining a growing interest by academic and industrial groups in the last few years: in organic photovoltaics, absorption in the NIR zone of the electromagnetic spectrum, indeed, affords an enhanced solar photons harvesting ability and a resulting increased efficiency;[25–29] they can also find useful application in the fields of semi-transparent solar cells[30] and photodetection as NIR organic photodiodes.[31] NIR absorbing materials are moreover emerging as interesting candidates for application as photothermal agents in cancer treatment.[6,32]

In this context, we report here three novel DPP based molecules, whose chemical structure is reported in Scheme 1.

The molecules are constituted by an electron poor DPP core N-functionalized with a bulky octyl-dodecyl tail and symmetrically linked to electron rich bithiophene moieties; the three molecules are end-capped with three different auxiliary electron acceptor groups so that a final A'-D—A—D—A' structure is achieved (with A' and A standing for acceptor and D for donor groups, respectively). This kind of molecular structure has been recently proved very useful in realizing efficient NFA molecules.[33] The choice, in our case, of a non-fused system based on a DPP core, whose chemistry is well established, and on commercial auxiliary acceptor terminal groups (A'), stems from the idea of reducing synthetic complexity. A similar approach can be found in recent literature works on thienyl-

substituted DPP derivatives, with promising results both in the fields of organic transistors and organic photovoltaics.[34–36] The novelty in the present work regards the use of different A' groups, specifically a thiobarbituric acid (TB), an indandione (ID) and a dicyanovinyl functionalized indandione (IDM). These terminal units, characterized by a different electron-acceptor strength, are expected to modulate the electronic properties at a molecular level and the microstructure in the solid/film phase. Regarding the donor part of the molecule, the bithiophene moiety was chosen also to allow a direct comparison with similar dyes bearing bi-furan moieties as donor groups that we reported in 2021.[37]
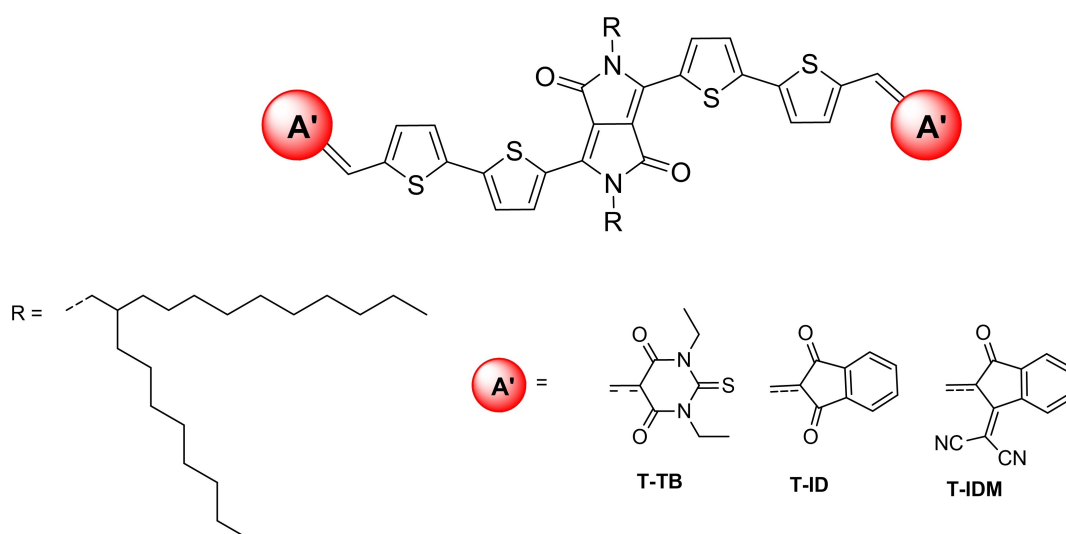
All the dyes were thoroughly characterized in terms of their structural, optical, thermal and electrochemical properties. A better insight into the electronic properties of the dyes has been achieved by means of a computational analysis performed at DFT level. A clear trend between the strength of the auxiliary electron acceptor group and some dye's properties as optical absorption maxima and frontier orbital's energies, was found. All the dyes are characterized by high molar extinction coefficients and optical absorption extending significantly in the NIR zone of the spectrum, especially in film phase. The compounds were finally processed as thin films and used as active layers in OFET to investigate their charge transport properties and promising results were obtained.
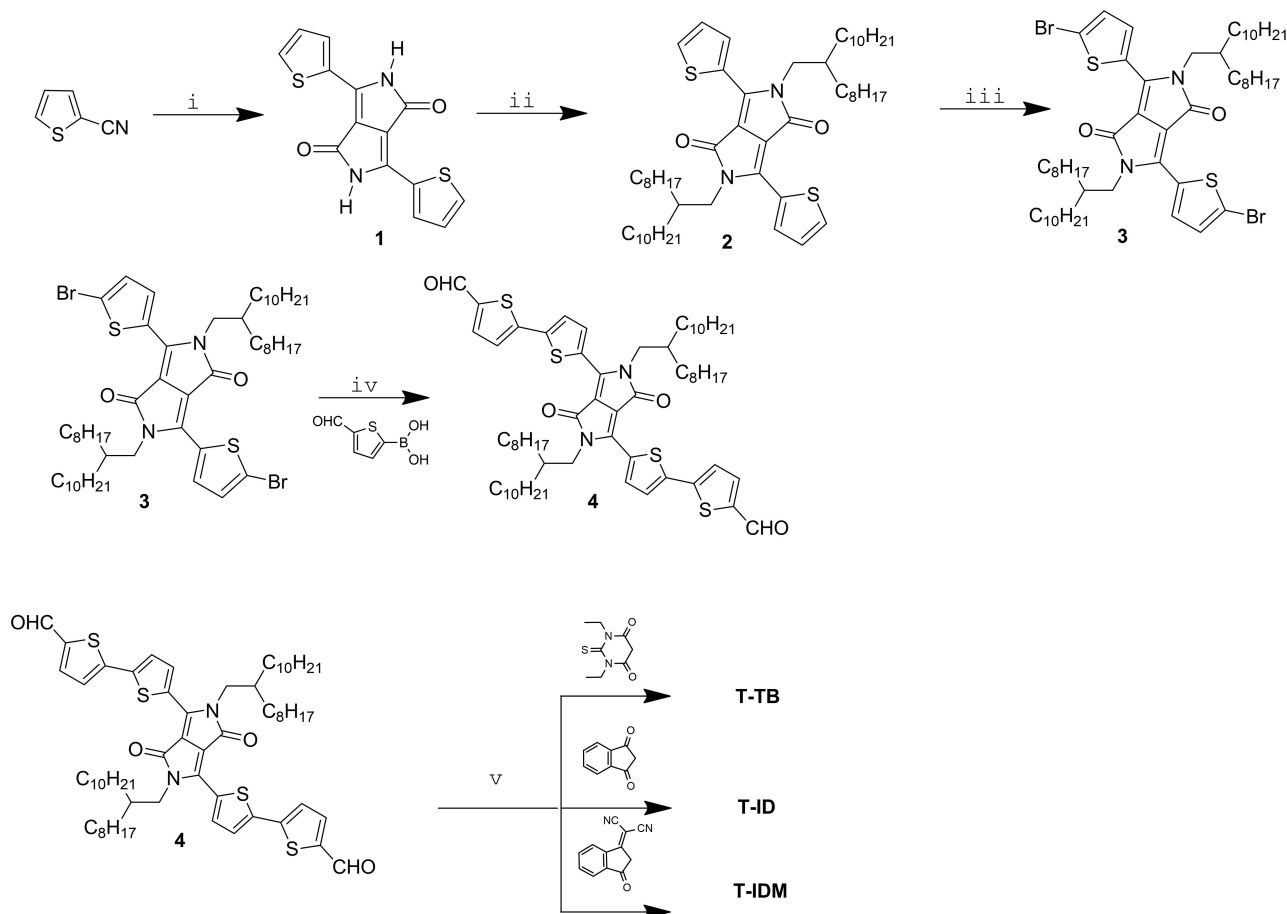
Results and Discussion

Chemical physical characterization

The novel DPP dyes were synthesized through a multistep synthetic procedure that is graphically sketched in Scheme 2.

DPP unit was obtained by the typically exploited succinic strategy:[1] 2-cyanothiophene was reacted with diisopropylsuccinate in a strongly basic environment at 130 °C and product 1

Scheme 1. Chemical formula of the synthesized dyes

Chemistry–A European Journal

Research Article
doi.org/10.1002/chem.202104552

Chemistry Europe
European Chemical
Societies Publishing

Scheme 2. Synthetic procedure followed for the preparation of the dyes; i) Na (1.3 equiv.), FeCl$_3$, di-isopropylsuccinate (0.8 equiv.) in t-amyl alcohol, 130 °C, 3 h, run in N$_2$; ii) Na$_2$CO$_3$, 1.5 equiv. of 1-bromo-2-octyldodecane, DMF, 130 °C, run in N$_2$, 20 h; iii) 1.1 equiv. of N-bromosuccinimide, chloroform, in the dark, run in N$_2$, RT, 16 h; iv) 2 equiv. of 5-formyl-2-thienylboronic acid, Pd$_2$(dba)$_3$, P(t-Bu)$_3$ x HBF$_4$, dry THF, N$_2$, reflux, 20 h; v) 2 equiv. of acceptor, dichloroethane-ethanol 4:1, β-alanine, reflux, 20 h, run in N$_2$.

was obtained with 80% yield. 1 was then N-functionalized through the reaction 1-bromo-2-octyldodecane (in turn prepared from the reaction of the corresponding alcohol with bromine/PPh3 in a classical Appel reaction) at high temperature in dimethylformamide (DMF) and in presence of K$_2$CO$_3$ as base, with 28% yield. This reaction is known to occur with low-to-moderate yield; one of the secondary products formed was identified to be the 9-methylene-nonadodecane, alkene deriving from the de-hydrobromination of 2-octyldodecylbromide characterized by diagnostic NMR resonance at 4.7 (singlet) and 2 (triplet) ppm.[38] This undesired product made tacky the recovered solid, but it could be easily removed by recrystallization in hot ethanol. Crystalline 2 was then reacted in the dark with N-bromosuccinimide (NBS) to obtain dibromo derivative 3 with 65% of yield after purification. A cross-coupling Suzuki reaction among 3 and 5-formyl-2-thienylboronic acid using Pd$_2$(dba)$_3$ as catalyst and p-(tBu)$_3$-HBF$_4$ as cocatalyst afforded the desired derivative 4 with high yield and a purity sufficiently high to use it in the next reaction without any purification step. This common diformyl precursor was finally functionalized with three different acceptor groups to afford the final DPP dyes: the

last synthetic step consisted in a Knoevenagel condensation of 4 with compound containing acid methylene group, specifically N,N-diethyl thiobarbituric acid (**T-TB**), indandione (**T-ID**) or 1,1-dicyanomethylene-3-indanone (**T-IDM**). β-alanine was used as catalytic base in this condensation reaction. The dyes were purified by Soxhlet extraction in methanol and acetone; the residues in the thimble were recovered finally by using chloroform as Soxhlet solvent.

NMR and ESI-MS analysis confirmed the expected molecular structures (see Figure S1–S9); in particular, 1H NMR analysis provided an indication of the relative strength of the auxiliary terminal acceptor groups of the four dyes. In particular, the resonance value of the proton of the methine group is influenced by the adjacent electron acceptor moiety: values of 8.63, 7.88 and 8.77 ppm were found for, respectively, **T-TB**, **T-ID** and **T-IDM**; this trend suggests that the electron acceptor strength is in the order **T-ID** < **T-TB** < **T-IDM**.

Thermal properties of the dyes were investigated by means of DSC and TGA analysis and are summarized in Table 1. DSC scans, reported in Figures S10–S12, showed that all the dyes are crystalline with a sharp melting point at 258, 264 and 280 °C

Chemistry–A European Journal

Research Article
doi.org/10.1002/chem.202104552

Chemistry Europe
European Chemical
Societies Publishing

Table 1. Thermal and optical properties of DPP dyes.							
Dyes	$T_m(°C)$[a]	$T_d(°C)$[b]	λ_1/λ_2 (nm)[c]	$\varepsilon_1/\varepsilon_2$ (cm^{-1}·M^{-1})[c]	E_g (eV)[d]	$\lambda_1/\lambda_2^{FILM}$ (nm)[e]	E_g^{FILM} (eV)[f]
T-TB	258	355	678/ 467	$9.51·10^4$/ $7.22·10^4$	1.54	726/ 820	1.43
T-ID	264	386	659/ 458	$7.76·10^4$/ $5.46·10^4$	1.60	724/ 848	1.32
T-IDM	280	370	714/ 488	$1.02·10^5$/ $4.35·10^4$	1.46	798/ 898	1.28

[a] Melting temperature determined by DSC analysis at 10°C min^{-1} under nitrogen atmosphere; [b] decomposition temperature determined as the temperature corresponding to the 5% weight loss of the samples in TGA measurement performed at 20°C min^{-1} in air; [c] UV-Vis spectra recorded in chloroform solution; [d] optical bandgap is determined as $1240/\lambda_{abs}^{onset}$ eV;[39] [e] UV-vis spectra recorded on film obtained by 1,1-2,2-tetrachloro-ethane solution by spin coating and thermally annealed at 110°C for 1 h; [f] optical bandgap calculated from the Tauc plot[40] of thermally annealed thin films.

respectively for **T-TB**, **T-ID** and **T-IDM**. The thermal stability of the dyes was assessed by TGA analysis: all the dyes featured a noteworthy thermal stability in air with decomposition temperature ranging from 355°C (**T-TB**) to 386°C (**T-ID**). TGA scans are reported in Figures S13-S15.

All the dyes were characterized regarding their optical properties both in solution and as thin films, with the results summarized in Table 1. Dye's UV-Vis absorption spectra in chloroform solution are presented in Figure 1.

Qualitatively, all the dye's solutions are characterized by two main optical features in the visible part of the spectrum. The more intense absorption peak is in the red zone of the spectrum with absorption maxima wavelength at 678, 659 and 714 nm for, respectively, **T-TB**, **T-ID** and **T-IDM**. The absorption at such high wavelengths is related to the peculiar molecular structure constituted by an alternation of electron acceptor and electron donor groups. Absorption wavelengths are clearly influenced by the terminal electron acceptor groups functional-izing the common molecular fragment: in particular, as the strength of the electron acceptor end group increases, the dye's absorption moves to higher λ values. As shown in previous papers,[41,42] functionalizing a specific molecular fragment with

electron acceptor groups of different strength has a relevant effect on tuning optical absorption properties of the molecular systems, occurring mainly through the stabilization of LUMO energies of the dyes. A second absorption occurs in the middle part of the spectrum (centred at a λ_2 value around 470 nm). This less intense optical feature eventually contributes to the final colour of the solutions, which is green for all the dye's solution (see Figure S16). Quantitatively, all compounds are characterized by noteworthy molar extinction coefficients ranging from $7.76·10^4$ (**T-ID**) to $1.02·10^5$ cm^{-1}·M^{-1} (**T-IDM**) as shown in Table 1.

The dyes were processed as thin films by spin coating from a solution of tetrachloroethane (5 mg/ml). The as casted films were then thermally annealed at 110°C (in accord with the procedure used for the deposition of the dyes in the fabrication of the organic filed effect transistors, OFET). UV-Vis absorption spectra of these films were recorded and are shown in Figure 1. Dye's thin films optical absorption is clearly red shifted as compared to solution as a consequence of the intermolecular interactions that occur in the solid state and the increased molecular order. The red-shift is particularly evident for **T-ID** and a possible explanation is linked to the higher symmetry and planarity of the indandione terminal groups (compared to the terminal groups functionalizing **T-IDM** and **T-TB**) that could help the crystal packing. For all the dyes, however, the absorption extends significantly in the NIR part of the spectrum. The thin films are characterized by two optical features beyond 700 nm: as reported on previous papers on similar DPP derivatives the low-energy feature could be assigned to the $0 \rightarrow 0$ vibronic component of the $\pi-\pi*$ transition while the higher energy one to the $0\rightarrow1$ transition.[43] While I_{0-0} absorption peak in the NIR is more intense than I_{0-1} for **T-ID**, the reverse occurs for **T-TB** and **T-IDM**. As shown in recent works by Spano,[44] the differences observed in the intensity ratio of these two vibronic peaks could be related to two different types of aggregates (H or J) when the strength of the intermolecular (excitonic) coupling is similar to the vibronic coupling. The different optical behaviour of **T-ID** as compared to **T-IDM** and **T-TB** can therefore be ascribed to a different microstructure formed in the film deposition. It was possible to evaluate the optical bandgap of the dyes as thin film through the Tauc's Plot methodology (see
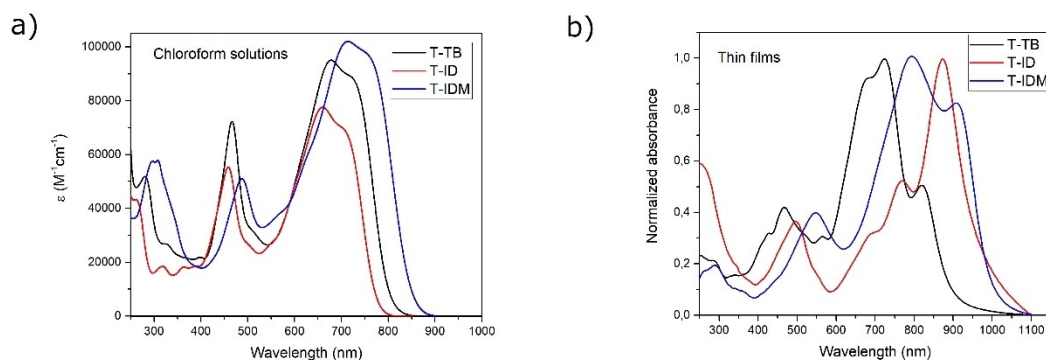

Figure 1. Molar extinction coefficients vs. wavelength for chloroform solutions of the reported dyes (a) and optical spectra of dye's thin films spin coated by 1,1-2,2-tetrachloroethane (b).

Chemistry–A European Journal

Research Article
doi.org/10.1002/chem.202104552

**Chemistry
Europe**

European Chemical
Societies Publishing

Figure S17–S19):[40] all the dyes are characterized by optical bandgap lower than 1.43 eV, which makes them very promising candidates for application in the field of organic photovoltaics and NIR organic photodetectors. In particular, **T-IDM** shows an extremely low bandgap value of 1.28 eV.

The dyes were electrochemically characterized by means of cyclic voltammetry (CV). The experiments were carried out in dichloromethane solution. CV is the technique of election to monitor the electroactivity of molecular species. Indeed, the first oxidation (reduction) potential of a molecule could be related to the energy level of its frontier molecular orbital, i.e. HOMO (LUMO). The determination of the latter is of pivotal importance when optoelectronic applications are conceived for the molecules under investigation. In the present context, the CVs of the different molecule were performed (Figure 2) and the extracted data are summarized in Table 2.

All the samples present a similar behaviour, showing multiple (quasi-reversible) peaks in the oxidation scan and almost flat voltammograms in the reduction scan (except for the solvent reduction at $V < -1.0\ V$). It was possible to obtain HOMO energy values from the oxidation potential (calculated as the $E_{1/2}$) by using the following equation:[45]

$$E_{HOMO} = -\left(E_{ox\ vs\ Fc^+/Fc} + 5.10\right)\ (eV) \tag{1}$$

The calculated values are quite similar, pointing out that the contribution to the HOMO is mainly due to the central (invariant) core of the molecules. A certain trend is anyway observed with HOMO energy values slightly decreasing as the
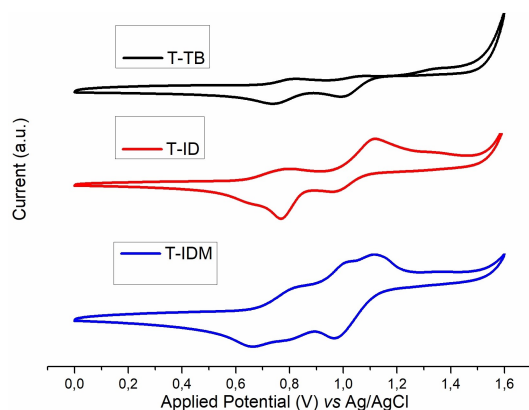
strength of the terminal acceptor groups increases, i.e. in the order **T-IDM** ($-5.87\ eV$) < **T-TB** ($-5.85\ eV$) < **T-ID** ($-5.81\ eV$). Unfortunately, from the reduction scans (not shown), no peaks could be (clearly) evidenced preventing us from calculating an "electrochemical" LUMO. Yet, a common approach to extract this value is to make use of the optical band gap adding it to HOMO energy in order to obtain LUMO energy: calculated optical bandgap (in dichloromethane solution) values of 1.55, 1.60 and 1.46 eV were found for **T-TB**, **T-ID** and **T-IDM**, respectively. By using these values, we could calculate LUMO energy values of -4.30, -4.21 and $-4.41\ eV$ respectively. In this case, the influence of the strength of the terminal acceptor groups is more accentuated: as the latter increases a significant stabilization of LUMO energies is observed.

DFT analysis

To get more information about the electronic structure of the synthesized dyes, a careful computational analysis was carried out at DFT level. The DFT-PCM geometry optimization procedure, that was carried out without any structural constraint, led to highly symmetrical structures in all case. Indeed, the final geometry of the molecules, (the long alkyl chain stretching away along the DPP nitrogen-nitrogen line is here modelled as a methyl group) could be described as a "quasi"-planar S-shaped arrangement with the planar DPP core in the middle. The optimized configurations, neglecting the tiny numerical differences in the coordinates that increase slightly with the complexity of substituents from **T-ID** to **T-TB**, belong to C2 point group symmetry. The most relevant deviation from planarity observed in the optimized structures regards the two pairs of thiophene rings that appear to be tilted with respect to each other and to the central DPP core, with the following dihedral angles: S–C–C–S (-169.73; -171.11; -169.08 degrees) and S–C–C–N (164.76; 165.61; 165.10 degrees) for **T-ID**, **T-IDM** and **T-TB**, respectively.

The predicted absorption spectra, reported in Figures S20–22, are consistent with the experimental ones. Wavelengths, energy, oscillator strengths (larger than 0.1) and percent contribution (larger than 10%) of a given transition between ground state orbitals to the excited state[46] are reported in Table S1. The theoretical spectrum in the fifty-excitation range explored by TD-DFT is made up of four (**T-ID**)/five (**T-IDM** and **T-TB**) principal bands, the highest one basically corresponding to HOMO→LUMO transition. In Table 3 we report information about these main transitions as well as dipole moments of the ground states and of the excited states, HOMOs and LUMOs energies and the optical band gap obtained from the TD-DFT vertical transition (E_g). The latter are in good agreement with the values extrapolated from experimental spectra ($\Delta E < 0.2\ eV$, see Table2) thus validating the calculation and the choice of the density functional.

As can be noticed in Table 3, the chromophores **T-ID** and **T-TB** show a consistent increase in the overall dipole moment values when passing from ground to excited state, whereas an equivalent decrease is predicted for **T-IDM**. A word of caution is

Figure 2. CV graphs of the synthesized dyes in dichloromethane solution

Table 2. Electrochemical potentials vs. Fc^+/Fc and estimated HOMO and LUMO energies vs. vacuum.

Dyes	E_{ox1}(V)[a]	HOMO (eV)[b]	E_g^{OPT} (eV)[c]	LUMO (eV)[d]
T-TB	0.75	-5.85	1.55	-4.30
T-ID	0.71	-5.81	1.60	-4.21
T-IDM	0.77	-5.87	1.46	-4.41

[a] Calculated as the half wave potential of the anodic and cathodic peaks; [b] calculated according to Ref. [45]; [c] optical bandgap is determined as $1240/\lambda_{abs}^{onset}$ eV;[39] [d] calculated by using the experimentally determined optical bandgap.

Chem. Eur. J. **2022**, *28*, e202104552 (5 of 12)

© 2022 The Authors. Chemistry - A European Journal published by Wiley-VCH GmbH

Chemistry–A European Journal

Research Article
doi.org/10.1002/chem.202104552

**Chemistry
Europe**
European Chemical
Societies Publishing

Table 3. Computed electronic and optical properties of the synthesized dyes.

Dyes	λ_{abs} (nm)	F[a]	Contributions	μ (GS)[b] (Debye)	μ (ES)[c] (Debye)	HOMO (eV)	LUMO (eV)	E_g (eV)
T-TB	771.62	2.24	H->L (98%)	1.52	1.99	−5.72	−3.62	1.61
T-ID	752.33	2.20	H->L (98%)	0.36	0.93	−5.61	−3.47	1.65
T-IDM	824.47	2.39	H->L (97%)	3.97	3.47	−5.70	−3.72	1.50

[a] oscillator strength; [b] computed ground state dipole moment; [c] computed first excited state dipole moment

Table 4. Hole-electron interaction analysis results

Dyes	S_r(a.u.)	D index(Å)	H index(Å)	t index(Å)	E_c (eV)[a]
T-TB	0.741	0.149	6.731	−0.860	2.899
T-ID	0.757	0.176	6.635	−0.643	2.906
T-IDM	0.680	0.158	7.538	−0.689	2.626

[a] Coulomb attractive energies between holes and electrons

necessary: the most important components of the dipole moment vector lie on an axis approximately orthogonal to the DPP plane (Z-axis) whereas, given the symmetry of the molecule, the components along the Y-axis, which corresponds to the DPP nitrogen-nitrogen line, and those along the X-axis directed along the molecular backbone direction, are close to zero. For what concerns HOMO and LUMO energies the trend is consistent with the values experimentally estimated by cyclic voltammetry analysis (see Table 2).

To gather deeper insight from the analysis of the variation of the electron density upon the main transition, the molecular structure of the three dyes was divided in five fragments, namely the central **DPP** core, two pairs of equivalent bi-thiophene rings (**BT1/2**) and two pairs of equivalent terminal acceptor groups (**A1/2**), the latter being specific to each system, while DPP core and bi-thiophene groups are shared by every molecule (see Figure S23 for a sketch of this partitioning). This partitioning was employed to perform a series of analyses: in the first one, the partial charges of all the atoms were calculated from the electron density of ground and excited states according to Mulliken partitioning scheme, and finally summed up for each fragment (table S2). The inspection of table again confirms that the first two molecules are highly symmetric, while **T-TB** optimized geometry is a bit further away from C2 point group. In all the molecules, the charge of the central **DPP** group is positive and the terminal groups are negatively charged, while the central bi-thiophene rings have smaller charges, either positive or negative. In the excited state, the Mulliken analysis predicts in all cases an increase of the charge on the central moiety. In addition, the more refined Inter-Fragment Charge Transfer (IFCT) analysis, confirmed the charge trend observed with Mulliken charges and showed that the central fragment transfers 0.267 electrons in **T-ID**, 0.357 in **T-IDM** and 0.278 in **T-TB** to the surrounding fragments (see Table S3). Both the analyses suggest that upon excitation electron density is transferred from the centre of the molecule towards the periphery. Finally, the full assessment of the Hole-Electron spatial distribution (Table 4) was carried out on the excited states TD-DFT wavefunctions by the Multiwfn program.[47,48] By this approach different quantities can be

calculated and discussed. The H index is an overall measure of the average spatial extension degree of hole and electron distribution based on their root-mean-square deviations (RMSDs). The D index is the total magnitude of charge transfer (CT) length as measured by the distance between the centres of mass of electrons and holes. The t index measures the separation degree of hole and electron in CT direction with negative values implying that the holes and electrons are not substantially separated due to CT. The S_r index defines the overlapping extent of holes and electrons. All the computed parameters indicate that the three studied transitions show a large overlap of electron and hole spatial distributions (Sr ≥ 0.680) and a small delocalization as pointed out by low D (less than one bond length) and (negative) t indexes. All these indicators suggest that the three transitions have very low charge transfer character and should be described as local excitations. This issue complies nicely with the high symmetry of the molecules, that can allow only multidirectional/centro-symmetric or intramolecular charge transfer. Among the three dyes, **T-IDM** shows the lowest exciton binding energy (defined as the calculated Coulomb integral between hole and electron distributions) and the largest delocalization, that is reflected in the largest electron transfer from the DPP center to the terminal substituents.

The latter phenomenon can be appreciated, as well, by inspecting the differential electron distribution maps between excited and ground states (difference densities) which are depicted in Figure 3 for all the chromophores. In the picture, the green lobes correspond to positive values of the difference ES–GS, i.e. larger values in the excited state, while the magenta surfaces correspond to negative ones-electron depletion in the excited state.

Notwithstanding the great overall similarity, some small differences can be pinpointed. In **T-IDM** surfaces, in particular, the green lobes extend furthest away from the centre, reaching the indole ring carbon atom near the di-cyanovinyl substituents, while in the other two molecules (at the same surface isovalue) the same distance, in terms of number of bonds, is not travelled. The reason for this behaviour most probably lies in the electron-withdrawing character of the dicyanovinyl fragment, that favours the deformation of electron cloud by "pulling" it towards the indandione ring. Another clue corroborating this interpretation can be found in the analysis of HOMO and LUMO densities of the ground states, that are shown in Figure S24. The picture clearly shows that in **T-IDM** LUMO a large density accumulation can be observed in the indandione ring around the dicyanovinyl substituent.
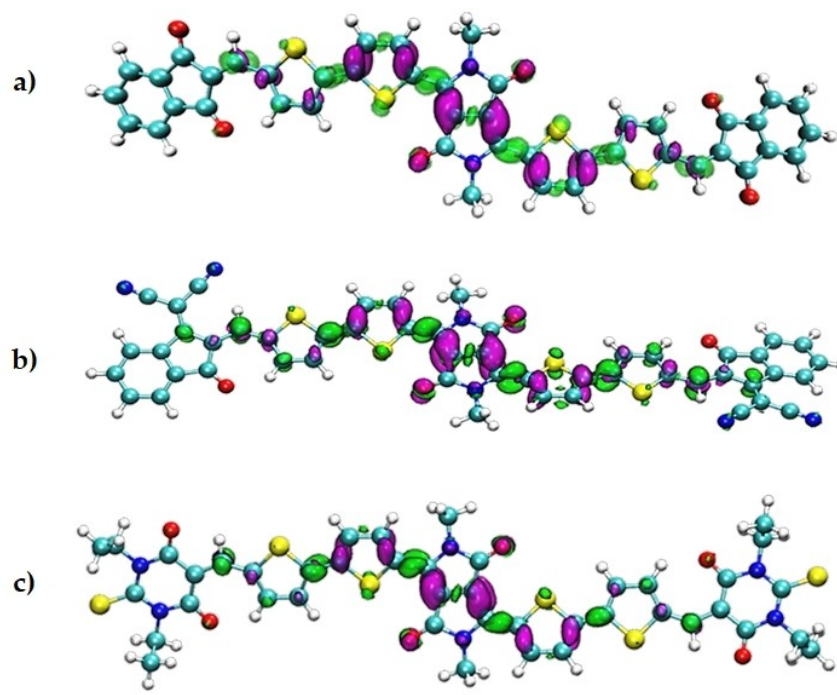
Figure 3. Magenta: negative density values; green: positive density values for a) **T-ID**; b) **T-IDM**; c) **T-TB**. (For interpretation of the references to colour in this figure legend, the reader is referred to the Web version of this article.)

Electrical characterization

The electrical response of the transistors bearing active channels spin-coated from the synthesized compounds was investigated by performing both transfer- (I_{DS} vs. V_{GS} at fixed V_{DS}) and output (I_{DS} vs. V_{DS} at fixed V_{GS}) curves. In particular, transfer-curves in the saturation regime ($V_{DS} = +$ or $-50\ V$) were employed to extract the field-effect mobility and threshold voltage values by the MOSFET equation used to fit linearly the square root of the measured I_{DS}:

$$\sqrt{I_{ds}} = \sqrt{\frac{W}{2L}C_{diel}\mu^*}(V_{GS} - V_{th}) \tag{2}$$

Here, μ and V_{th} represent the mobility and the threshold voltage, respectively, while C_{diel} is the dielectric oxide capacitance per unit area being here equal to 17.25 nF/cm^2. Transfer and output curves of the dye's based OFET are shown in Figure 4.

According to our analysis, all the investigated compounds are able to exhibit an ambipolar field-effect behavior, meaning that the I_{DS} current can be enhanced upon the application of both positive and negative V_{GS} voltages. However, for each compound, the field-effect response was found to be considerably stronger for one of the two carrier types (i.e. holes or electrons). This occurrence is clearly summarized in Table 5 which presents the mobility and the threshold voltage values extracted from the transfer curves recorded in the saturation regime. Here, mean values were achieved by considering at least four transistors for any molecule, with the error bars representing the standard deviation values. As shown in Figures 4a–b–c, in general, a very small hysteresis was observed in the output curves where the differences between the current values measured in the forward (from the off to the on region) and backward (from the on to the off regions) sweeps are hardly discernible. Given its negligible impact on the overall response evaluation, this feature was not systematically analyzed for all the investigated devices. Conversely, much

Table 5. Electron and hole mobility (μ) and threshold voltage (V_{th}) values estimated by Equation2 for the transistors based on the investigated single dyes and on the **IDM/ID** blend.

Dyes	μ_e^{aver} (cm^2/V s)	μ_e^{max} (cm^2/V s)	$V_{th,e}^{Avg}$ (V)	μ_h^{aver} (cm^2/V s)	μ_h^{max} (cm^2/V s)	$V_{th,h}^{Avg}$ (cm^2/V s)
T-TB	$(1.9 \pm 0.9) \cdot 10^{-4}$	$2.9 \cdot 10^{-4}$	-9.5 ± 3.3	/	$< 1.5 \cdot 10^{-6}$	/
T-ID	$(5.9 \pm 5.0) \cdot 10^{-5}$	$1.4 \cdot 10^{-4}$	29.5 ± 3.0	$(1.3 \pm 0.7) \cdot 10^{-3}$	$2.3 \cdot 10^{-3}$	-6.0 ± 4.5
T-IDM	$(3.6 \pm 0.7) \cdot 10^{-2}$	$4.4 \cdot 10^{-2}$	22.5 ± 0.6	$(5.4 \pm 2.0) \cdot 10^{-4}$	$8.2 \cdot 10^{-4}$	-16.5 ± 2.0
ID/IDM blend[a]	$(0.9 \pm 0.3) \cdot 10^{-3}$	$1.2 \cdot 10^{-3}$	24.1 ± 3.0	$(1.7 \pm 0.7) \cdot 10^{-3}$	$2.4 \cdot 10^{-3}$	-27.4 ± 3.0

[a] The **ID/IDM** blend consists of a thin film deposed by a solution containing 50:50 wt of **T-ID** and **T-IDM**.

Chemistry–A European Journal

Research Article
doi.org/10.1002/chem.202104552

Chemistry
Europe
European Chemical
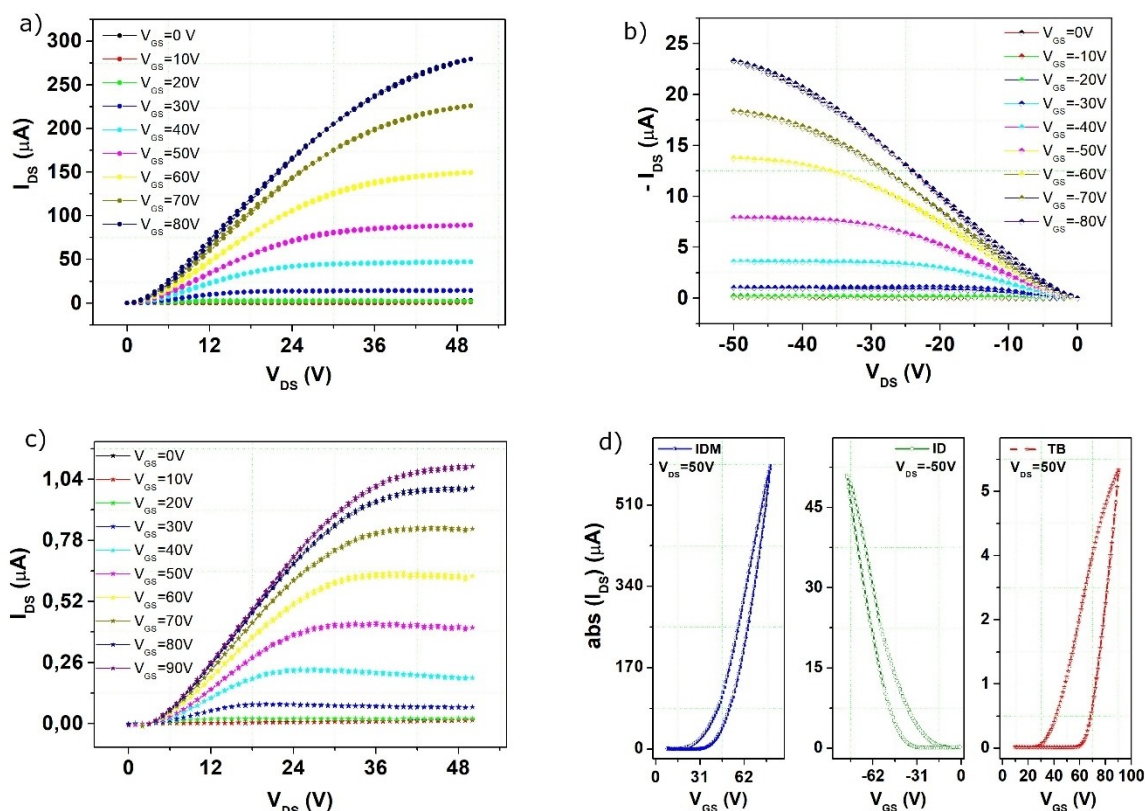Societies Publishing

Figure 4. Output curves measured for transistors based on a) **T-IDM**, b) **T-ID**, c) **T-TB** molecules; d) Corresponding transfer curves acquired in the saturation regime. All these curves are referred only to the majority carrier response for any compound.

more evident was the hysteresis manifestation in the transfer curves (Figure 4d) featuring the typical anticlockwise shape (i.e. current in the forward sweep is larger than in the backward sweep). As widely reported in the literature, this phenomenon can be associated to the occurrence of charge trapping mechanisms being ascribable both to the intrinsic structural disorder in the semiconducting layers and/or to the action of spurious chemical species (i.e., water molecules) still present on SiO_2 surface.[49]

Table 5 presents the mobility and the threshold voltage values extracted from the transfer curves recorded in the saturation regime. In this case, as commonly reported in the literature, only the current curves recorded in the forward sweep were considered for the parameter estimation. It should be outlined that mean values in Table 5 were achieved by considering at least four transistors for any molecule, with the error bar representing the standard deviation values.

As a whole, Table 5 reveals that the **T-IDM** molecule is the most promising in terms of the field-effect performances. This compound is characterized by a strongly dominant n-type character with a maximum electron mobility approaching 0.05 cm²/V·s. Significantly, the related averaged electron mobility was estimated to be larger by almost two orders of magnitude than the corresponding hole mobility. The opposite situation was observed for the **T-ID** compound which is mainly a hole-transporting (p-type) semiconductor. For this molecule,

indeed, hole mobility values are by far (i.e. at least one order of magnitude) higher than those of electrons. Finally, similar to **T-IDM**, the **T-TB** dye exhibited a more pronounced n-type behavior even if with a significantly reduced electron mobility. For **T-TB**, moreover, the hole-accumulation phenomenon was not clearly detected for all the investigated devices and only an estimation of the maximum hole mobility value (10^{-6} cm²/V s) could be thus achieved. Figure S25 reports, for any investigated compound, the best transfer curve in the saturation regime obtained for the minority carrier (i.e. carrier type with the smaller mobility values). In the same Figure, the output curves measured for **T-IDM** in the hole accumulation region are also shown. These clarify how, for small V_{GS} and high V_{DS} (both considered in absolute value), the device response is dominated by the injection of the majority carriers (electrons, in this case) from the drain electrode.

The different field-effect behavior of the dyes could in part be related to their electronic properties. In particular, considering the estimated HOMO and LUMO values as given in Table 2, for **T-IDM** and **T-TB** the electron injection barriers from gold electrodes ($W_f \approx 5.0$ eV for Au) should be smaller than those related to the hole injection, thus supporting the observed dominant electron-transporting response. Similar considerations should explain the opposite behavior occurring for **T-ID** featuring the higher values of both HOMO and LUMO. Anyway, charge transport behavior in organic semiconductors depends

Chemistry–A European Journal

Research Article
doi.org/10.1002/chem.202104552

Chemistry Europe
European Chemical
Societies Publishing

not only on the molecular structure but also on the micro-structure and morphology of the final solid-state assemblies. Hence, it is not possible to give an unequivocal explanation of the differences in charge transport properties without the exhaustive knowledge of the crystal structure of the analyzed dyes. Unfortunately, in this study, we did not manage to obtain single crystals of the latter suitable for the resolution of the structure. In Figure S26a, however, XRD spectra of dye's films obtained by drop casting are shown. For all the layers it was possible to observe a sharp peak at low 2θ value (d spacing around 18 Å), indicative of a lamellar organization and a broader peak at higher 2θ with d spacing around 3.5 Å (not visible for the **T-TB** drop casted film but still present in the XRD spectrum, of the bulk material, not shown) associated to the π-π stacking. In addition, the presence of an amorphous halo centered at $2\theta \approx 26°$ suggests a common semicrystalline nature for the films. As compared to the other two dyes **T-ID** is also characterized by several further peaks, suggestive of a different crystalline phase that could be the origin of the different charge transport behavior.

On the basis of the above discussed results and with the aim of getting a field-effect response with a more balanced ambipolar character (namely, with comparable electron and hole mobility values), an alternative transistor configuration was investigated by spin-coating active layers from a solution containing a **T-ID** and **T-IMD** in the same amount (**ID/IDM blend**). In comparison with the "single dye" devices, the same spin-coating parameters and thermal annealing protocol were employed.

Figure 5 shows the output and transfer-curves recorded for an **ID/IDM blend** device, confirming very clearly the improved ambipolar response achieved in this way. The maximum I_{DS} values were indeed comparable under the application of both positive and negative V_{GS} and these symmetric features can be directly ascribed to the similar values of electron and hole mobility as well as of the related threshold voltages. This general scenario is well described by the data reported in the last row of Table 5, summarizing the overall results achieved for the investigated set of the **ID/IDM blend**-based devices. As shown, maximum mobility values were larger than 10^{-3} cm^2/V·s

for both electrons and holes, with slightly better performances for the latter. As compared to **T-IDM** single layer devices electron mobility decreases by about one order of magnitude. This feature was in some way expected since electron (n-type) transport is typically (given the involved energy levels) a less robust process in organic semiconductors in comparison to p-charge transport, being so more affected by the overall surrounding environment. A larger electron mobility reduction in blend active channels was also reported in other recent works.[50,51]

Looking at the XRD spectrum of the blended layer (Figure S26a), it is possible to infer that the two dyes in the blend crystallize separately; this assumption is confirmed by UV-Vis analysis where the related optical spectrum (Figure S26b) is approximately the sum of the spectra of the two pure dyes as thin films (see Figure 1). A DSC analysis performed on the drop casted blend (Figure S26c) shows indeed two melting peaks even if at temperature lower than those of the two pure dyes. Further optimization of the field-effect response of these devices could be pursued in future by analyzing more carefully the impact of different concentrations for the two starting molecules.

Finally, for sake of completeness, the morphological features of typical active layers which were electrically characterized in this study, can be observed in Figure 6 where non-contact AFM topographies are reported. The **T-IDM** film clearly shows a structured morphology characterized by needle-like crystallites with an average length of 100 nm and 4 nm in height ($\sigma_{rms} \approx 2$ nm). Conversely, **T-ID** surfaces are decorated by the sparse presence of agglomerates as possible indication of a lower interaction with the HMDS-treated SiO$_2$ substrates. Interestingly, the **ID/IDM blend** shows (Figure 6d), at least on the surface, a more marked structuring with a compact corrugated surface.

Conclusions

We report here on the synthesis of three novel DPP derivatives and on their chemical physical, computational and electrical characterization. The molecular structure of the dyes is based
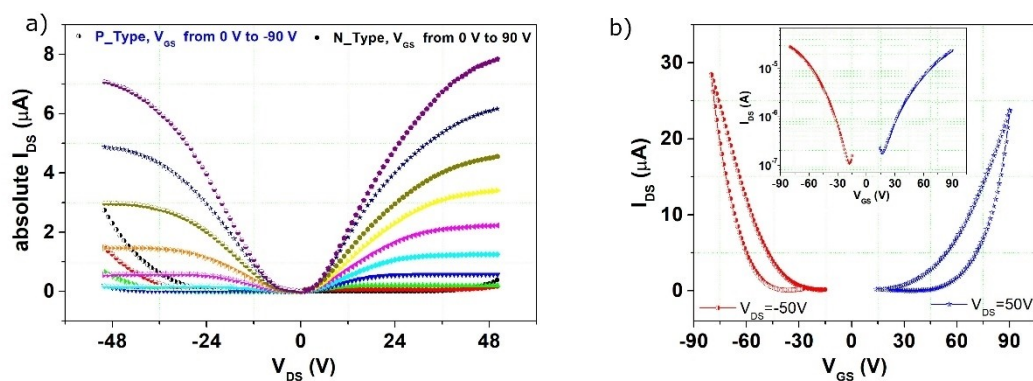
Figure 5. a) Output and b) transfer-curves in saturation regime achieved for an **ID/IDM blend** based transistor. In the inset of the b, the transfer-curves are reported in a semilog-plot.
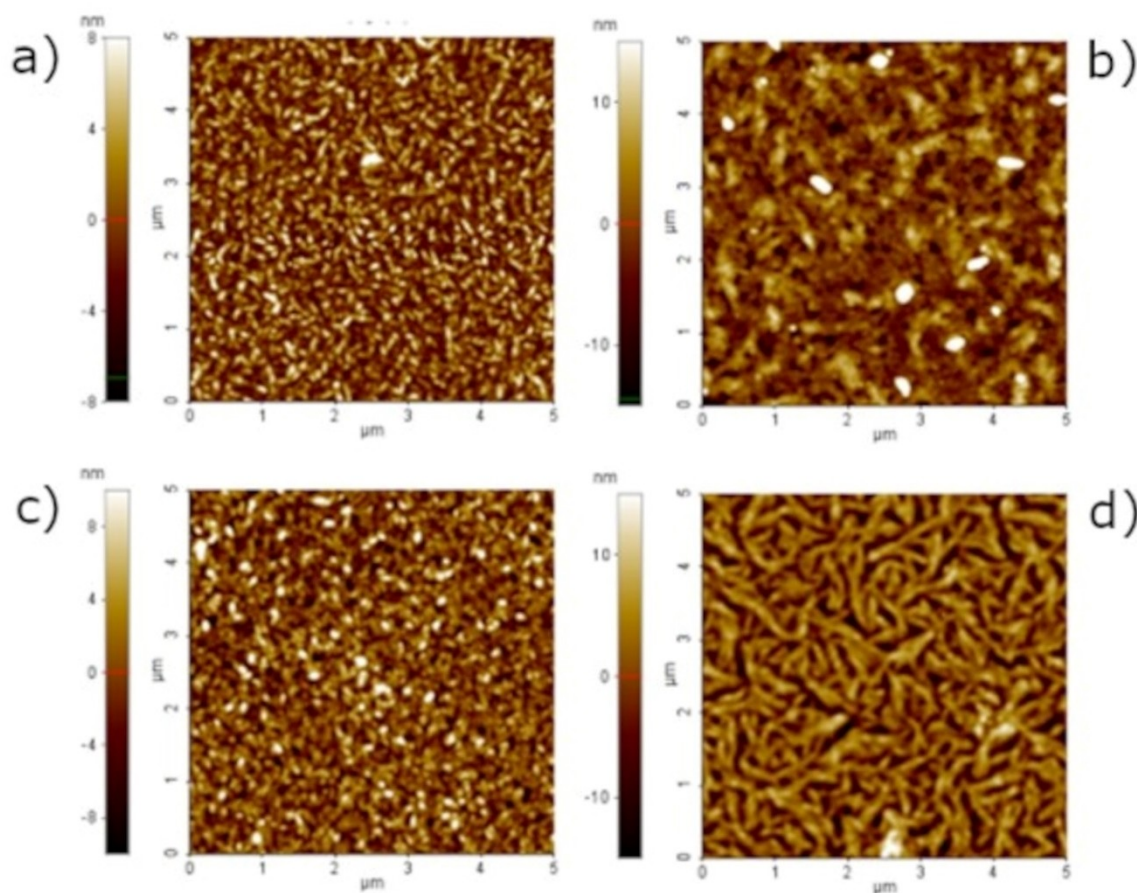
Chemistry–A European Journal

Research Article
doi.org/10.1002/chem.202104552

Chemistry Europe
European Chemical
Societies Publishing

Figure 6. Non-contact AFM topographies (5 x 5 μm^2, 512 x 512 pxl) of the active layers of the studied OFET devices: (a) **T-IDM**, (b) **T-ID**, (c) **T-TB**, d) **IDM/ID** blend

on a common molecular fragment, constituted by an electron acceptor DPP core, symmetrically coupled to two bithiophene donor moieties and end-terminated with auxiliary acceptor groups of different strength. All the dyes absorb at high wavelengths as a consequence of the alternation, along the molecular structure, of electron acceptor and donor groups. The wavelengths of the absorption maxima show a clear trend with the strength of the auxiliary acceptor groups: the higher the strength, the more red-shifted the optical maxima. Optical analysis performed on thin films display, as compared to solutions, a further red-shif of the absorption that extends significantly in the NIR zone of the spectrum. As thin films, the dyes exhibit narrow optical bandgaps ranging from 1.43 to 1.28 eV. An electrochemical characterization was carried out on dichloromethane solutions of the dyes: very stable HOMO energies were found consistently with the high thermo-oxidative stability of the dyes assessed by TGA analysis. As far as LUMO energies are concerned, they are very stable as well (energies below −4 eV), showing a clear trend with the strength of the auxiliary acceptor groups functionalizing the dyes. Electronic properties were investigated at DFT level and high-lighted a very low charge transfer in the main excitation with electron transfer moving from the core of the dyes towards the

periphery. In order to assess the charge transport performances, the synthesized dyes were finally used as active layers in the fabrication of OFET devices. Though all the molecules present a certain degree of ambipolarity, it has to be stressed that for each of them one type of charge transport is preferential. In terms of electric response, the best dye is **T-IDM** which show a dominant N-type response with a very interesting electron mobility up to $4.4 \cdot 10^{-2}$ cm^2/V·s; **T-TB** afforded, as well, N-type transistor with, anyway, a much lower mobility. The dye **T-ID** was instead found to be preferentially P-type with hole mobility values up to $2.3 \cdot 10^{-3}$ cm^2/V·s. Finally, a device featuring a blend of **T-ID/T-IDM** dyes as active layer was fabricated and a balanced ambipolar response, with comparable hole and electron mobilities in the order of 10^{-3} cm^2/V·s, was obtained.

Experimental Section

General procedures

All reagents were purchased by Sigma Aldrich or Alfa Aesar and used without any further purification, unless otherwise specified. All air- or moisture-sensitive reactions were carried out under nitrogen atmosphere. Details of the synthetic procedures are reported in

Chemistry–A European Journal

Research Article
doi.org/10.1002/chem.202104552

**Chemistry
Europe**
European Chemical
Societies Publishing

detail in the Supporting Information. The compounds' identity was confirmed by Varian Inova 500 and Bruker 400 MHz NMR spectrometers. GC-MSspectra were recorded on a Thermo Finnigan Trace GC with a cross-linked methyl silicone capillary column, coupled to a Thermo Finnigan Trace MS mass spectrometer equipped with an electronic impact source (EI). Thermogravimetric analysis (TGA) was carried by a TA4000 Perkin- Elmer instrument at a heating rate of $20\,°C\,min^{-1}$ under air in the temperature range $30–900\,°C$. The reported decomposition temperature refers to 5% weight loss. Differential scanning calorimetry (DSC) analysis was performed on a DSC Mettler 822e instrument under a nitrogen flow at a heating rate of $10\,°C\,min^{-1}$. Absorption spectra were recorded on Jasco V-530 UV-vis spectrophotometer at room temperature with a scanning rate of 200 nm/min. FTIR spectra were recorded dispersing the dye in KBr pellets and using a Thermofisher Nicolet 5700 FTIR spectrometer. Thin films of the dyes were prepared by spin-coating a chloroform solution of the dyes on glass substrates for optical characterization by means of a Laurell WS-650Mz-23NPP spin processor. Electrochemical characterization was performed by means of cyclic voltammetry (CV) using a BioLogic sp150 potentiostat. The samples were analyzed in dichloromethane solution in a three-electrode set-up, with a Au working electrode and a Pt wire counter-electrode while Ag/AgCl was used as the reference electrode. Electrolyte consisted in a tetrabutylammonium hexafluorophosphate 0.1 M solution in dichloromethane. CV were conducted at 100 mV/s. The found potential values were referred to Fc/Fc+ acting as internal standard. Before each measurement, the electrolyte was degassed with Argon to avoid the presence of oxygen. Thin films of the dyes obtained by drop casting a 5 mg/ml chloroform/1,1-2,2-tetrachloroethane solution (9/1 v/v) on a cover-slip microscope glass. The films were annealed for 1 h at $110\,°C$ and their X-ray diffraction profiles were obtained with a Philips PW1830 powder diffractometer, using Cu Kα radiation ($λ = 1.5418$ Å), by a continuous scan of the diffraction angle 2θ at a speed of $0.01°/s$.

DFT studies

The ground state electronic structure of the dyes was investigated using density functional theory (DFT), whereas the excited states and the UV-Vis absorption spectra were obtained with linear-response time dependent DFT (LR-TDDFT) calculations. The following hybrid functionals, differing by the Hartree-Fock exchange percentage, were employed in the initial phase, in order to evaluate the best performing one with the dyes investigated: CAM-B3LYP,[52] PBE0,[53] M06-2X;[54] the polarized 6–31+G(d,p) basis set was used in all the tests. The final choice was PBE0, owing to the good reproduction of experimental UV-Vis absorption patterns (peak position within 0.2 eV). The solvent effect of chloroform (static dielectric permittivity $ε = 4.711300$, dielectric permittivity at infinite frequency $ε(∞) = 2.090627$) was evaluated using the Polarizable Continuum Model (PCM) formalism (IEF variant), as implemented in the code Gaussian 16.[55] The long 2-octyldodecyl alkyl chains were replaced by methyl groups, and the structures of the molecules were optimized in a three-stage process, that includes first a Hartree-Fock relaxation with the same basis set using standard minimization techniques[56] followed by the DFT/PCM optimization and by the final time-dependent excitation analysis (vertical transitions) on the optimized geometry. To verify that the stationary points found were real minima on the potential energy surface, the calculation of the vibrational frequencies was carried out, and no imaginary values were found in any case.

All QM computations were performed with G16 package,[55] whereas the analysis of the percentage contributions to the calculated TD-DFT spectra was accomplished with the code GaussSum 3.0 51, by assigning a Gaussian function with Half-Width at Half Height (HWHH) equal to 0.2 eV (1613 cm^{-1}) to each vertical transition (line). The post-processing code MultiWfn[48] was used to perform further analyses of the wavefunction to gather information about the charge transfer in the transition.

Transistor fabrication and film characterization

For the transistor fabrication, thin films from the synthesized dyes were spin-coated on multilayer structures consisting of a 500-μm thick highly-doped silicon (Si++), working as substrate and gate electrode, a 200-nm thick SiO_2 dielectric barrier and 150-nm thick pre-patterned source/drain interdigitated gold electrodes, defining active channels with width/length (W/L) ratios of 550. In recent past, this device configuration was widely employed for the electrical characterization of several conjugated compounds with conductivity and field-effect mobility values down to 10^{-8} S/cm and 10^{-7} cm^2/V·s, respectively.[49,58]

For the spin-coating process, solutions of the dyes in 1,1-2,2-tetrachloroethane (5 mg/ml) were utilized. The solutions were spin-coated on the substrates at 1000 rpm for 1 minutes and then at 2000 rpm for 30 s. After the deposition, films were annealed in a vacuum oven, at $110\,°C$, for 1 h.

Before the film deposition, all multilayer Si++/SiO_2/Au substrates were functionalized by applying HMDS (hexamethyldisilazane) self-assembling monolayers in a such way to increase the SiO_2 surface water-contact angle ($θ_C$) up to ~110°.[59] This procedure allows strongly reducing the charge trapping phenomena related to residual water molecules absorbed on the SiO_2 surface.[60] All the electrical measurements were carried out in vacuum (base pressure P_r ~10^{-5} mbar) mounting the samples in a Janis cryogenic probe station, connected to a Keithley 4200 Semiconductor Parameter Analyzer. In this way, the gate-source (V_{GS}) and drain-source (V_{DS}) voltages could be applied contemporarily and the related I_{DS} and I_{GS} currents were measured in parallel.

The surface morphological features of the spin-coated films were characterized by Atomic Force Microscopy (AFM) in non-contact mode using a Park system XE100 microscope, equipped with PPP-NCHR silicon cantilevers (NanoSensors).

Conflict of Interest

The authors declare no conflict of interest.

Data Availability Statement

The data that support the findings of this study are available in the supplementary material of this article.

[1] N. Luo, G. Zhang, Z. Liu, *Org. Chem. Front.* **2021**, *8*, 4560–4581.

[2] M. Kaur, D. H. Choi, *Chem. Soc. Rev.* **2015**, *44*, 58–77.

[3] M. Grzybowski, D. T. Gryko, *Adv. Opt. Mater.* **2015**, *3*, 280–320.

[4] C. Zhao, Y. Guo, Y. Zhang, N. Yan, S. You, W. Li, *J. Mater. Chem. A* **2019**, *7*, 10174–10199.

[5] Q. Liu, S. E. Bottle, P. Sonar, *Adv. Mater.* **2020**, *32*, 1903882.

[6] X. Jiang, L. Wang, H. Tang, D. Cao, W. Chen, *Dyes Pigm.* **2020**, *181*, 108599.

[7] W. W. Bao, R. Li, Z. C. Dai, J. Tang, X. Shi, J. T. Geng, Z. F. Deng, J. Hua, *Front. Chem. (Lausanne)* **2020**, *8*, 679.

[8] D. G. Farnum, G. Mehta, G. G. I. Moore, F. P. Siegal, *Tetrahedron Lett.* **1974**, *15*, 2549–2552.

[9] O.Wallquist, R. Lenz, in *High Performance Pigments: Second Edition* (Eds.: E. B. Faulkner, R. J. Schwartz), WILEY-VCH Verlag GmbH & Co. KGaA, Weinheim, **2009**, p. 165.

[10] W. Li, K. H. Hendriks, M. M. Wienk, R. A. J. Janssen, *Acc. Chem. Res.* **2016**, *49*, 78–85.

[11] A. Tang, C. Zhan, J. Yao, E. Zhou, *Adv. Mater.* **2017**, *29*, 1600013.

[12] W. Li, W. S. C. Roelofs, M. Turbiez, M. M. Wienk, R. A. J. Janssen, *Adv. Mater.* **2014**, *26*, 3304–3309.

[13] Y. Kim, C. E. Song, E. J. Ko, D. Kim, S. J. Moon, E. Lim, *RSC Adv.* **2015**, *5*, 4811–4821.

[14] W. Zhang, K. Shi, J. Huang, D. Gao, Z. Mao, D. Li, G. Yu, *Macromolecules* **2016**, *49*, 2582–91.

[15] B. Lim, H. Sun, Y. Y. Noh, *Dyes Pigm.* **2017**, *142*, 17–23.

[16] A. Zhang, C. Xiao, Y. Wu, C. Li, Y. Ji, L. Li, W. Hu, Z. Wang, W. Ma, W. Li, *Macromolecules* **2016**, *49*, 6431–6438.

[17] N. Zhou, S. Vegiraju, X. Yu, E. F. Manley, M. R. Butler, M. J. Leonardi, P. Guo, W. Zhao, Y. Hu, K. Prabakaran, R. P. H. Chang, M. A. Ratner, L. X. Chen, A. Facchetti, M. C. Chen, T. J. Marks, *J. Mater. Chem. C* **2015**, *3*, 8932–8941.

[18] H. Zhang, R. Li, Z. Deng, S. Cui, Y. Wang, M. Zheng, W. Yang, *Dyes Pigm.* **2020**, *181*, 108552.

[19] Z. Yuan, B. Fu, S. Thomas, S. Zhang, G. Deluca, R. Chang, L. Lopez, C. Fares, G. Zhang, J. L. Bredas, E. Reichmanis, *Chem. Mater.* **2016**, *28*, 6045–6049.

[20] C. Y. Yang, W. L. Jin, J. Wang, Y. F. Ding, S. Nong, K. Shi, Y. Lu, Y. Z. Dai, F. D. Zhuang, T. Lei, C. A. Di, D. Zhu, J. Y. Wang, J. Pei, *Adv. Mater.* **2018**, *30*, 1802850.

[21] R. Di Pietro, T. Erdmann, J. H. Carpenter, N. Wang, R. R. Shivhare, P. Formanek, C. Heintze, B. Voit, D. Neher, H. Ade, A. Kiriy, *Chem. Mater.* **2017**, *29*, 10220–10232.

[22] G. Lin, Y. Qin, J. Zhang, Y. S. Guan, H. Xu, W. Xu, D. Zhu, *J. Mater. Chem. C* **2016**, *4*, 4470–4477.

[23] J. Yang, H. Wang, J. Chen, J. Huang, Y. Jiang, J. Zhang, L. Shi, Y. Sun, Z. Wei, G. Yu, Y. Guo, S. Wang, Y. Liu, *Adv. Mater.* **2017**, *29*, 1606162.

[24] H. Zhang, K. Yang, K. Zhang, Z. Zhang, Q. Sun, W. Yang, *Polym. Chem.* **2018**, *9*, 1807–1814.

[25] Y. Li, J. D. Lin, X. Liu, Y. Qu, F. P. Wu, F. Liu, Z. Q. Jiang, S. R. Forrest, *Adv. Mater.* **2018**, *30*, 1804416.

[26] S. Dai, T. Li, W. Wang, Y. Xiao, T. K. Lau, Z. Li, K. Liu, X. Lu, X. Zhan, *Adv. Mater.* **2018**, *30*, 1706571.

[27] H. Yao, Y. Cui, R. Yu, B. Gao, H. Zhang, J. Hou, *Angew. Chem. Int. Ed. Engl.* **2017**, *56*, 3045–3049.

[28] D. Yang, H. Sasabe, T. Sano, J. Kido, *ACS Energy Lett.* **2017**, *2*, 2021–2025.

[29] G. Li, W. H. Chang, Y. Yang, *Nat. Rev. Mater.* **2017**, *2*, 1–13.

[30] G. P. Kini, S. J. Jeon, D. K. Moon, *Adv. Funct. Mater.* **2021**, *31*, 2007931.

[31] X. Liu, Y. Lin, Y. Liao, J. Wu, Y. Zheng, *J. Mater. Chem. C* **2018**, *6*, 3499–3513.

[32] Q. Ma, X. Sun, W. Wang, D. Yang, C. Yang, Q. Shen, J. Shao, *Chin. Chem. Lett.* **2021**, https://doi.org/10.1016/J.CCLET.2021.10.054.

[33] J. Yuan, Y. Zhang, L. Zhou, G. Zhang, H. L. Yip, T. K. Lau, X. Lu, C. Zhu, H. Peng, P. A. Johnson, M. Leclerc, Y. Cao, J. Ulanski, Y. Li, Y. Zou, *Joule* **2019**, *3*, 1140–1151.

[34] Y. Eom, C. E. Song, W. S. Shin, S. K. Lee, E. Lim, *J. Ind. Eng. Chem.* **2017**, *45*, 338–348.

[35] A. Riaño, P. Mayorga Burrezo, M. J. Mancheño, A. Timalsina, J. Smith, A. Facchetti, T. J. Marks, J. T. López Navarrete, J. L. Segura, J. Casado, R. Ponce Ortiz, *J. Mater. Chem. C* **2014**, *2*, 6376–6386.

[36] S. Ghosh, R. Raveendran, A. Saeki, S. Seki, M. Namboothiry, A. Ajayaghosh, *ACS Appl. Mater. Interfaces* **2019**, *11*, 1088–1095.

[37] S. Fusco, M. Barra, M. Bonomo, A. Cassinese, R. Centore, F. Chiarella, F. Senneca, A. Carella, *Dyes Pigm.* **2021**, *186*, 109026.

[38] J. Wakabayashi, M. Gon, K. Tanaka, Y. Chujo, *Macromolecules* **2020**, *53*, 4524–4532.

[39] R. Li, M. Liu, S. K. Matta, A. Hiltunen, Z. Deng, C. Wang, Z. Dai, S. P. Russo, P. Vivo, H. Zhang, *Adv. Sustainable Syst.* **2021**, *5*, 2100244.

[40] C. Coluccini, N. Manfredi, M. M. Salamone, R. Ruffo, M. G. Lobello, F. de Angelis, A. Abbotto, *J. Org. Chem.* **2012**, *77*, 7945–7956.

[41] C. Maglione, A. Carella, R. Centore, S. Fusco, A. Velardo, A. Peluso, D. Colonna, A. di Carlo, *J. Photochem. Photobiol. A* **2016**, *321*, 79–89.

[42] M. Bonomo, A. Carella, F. Borbone, L. Rosato, D. Dini, L. Gontrani, *Dyes Pigm.* **2020**, *175*, 108140.

[43] M. Más-Montoya, R. A. J. Janssen, M. Más-Montoya, R. A. J. Janssen, *Adv. Funct. Mater.* **2017**, *27*.

[44] F. C. Spano, *Acc. Chem. Res.* **2009**, *43*, 429–439.

[45] C. M. Cardona, W. Li, A. E. Kaifer, D. Stockdale, G. C. Bazan, *Adv. Mater.* **2011**, *23*, 2367–2371.

[46] R. L. Martin, *J. Chem. Phys.* **2003**, *118*, 4775–4777.

[47] W. Zhuang, S. Wang, Q. Tao, W. Ma, M. Berggren, S. Fabiano, W. Zhu, E. Wang, *Macromolecules* **2021**, *54*, 970–980.

[48] T. Lu, F. Chen, *J. Comput. Chem.* **2012**, *33*, 580–592.

[49] M. Barra, F. Chiarella, F. Chianese, R. Vaglio, A. Cassinese, *Electronics (Switzerland)* **2019**, *8*, 249.

[50] S. Park, B. Lee, B. Bae, J. Chai, S. Lee, C. Kim, *Synth. Met.* **2019**, *253*, 40–47.

[51] I. Frac, M. Kucinska, P. Gawrys, M. Zagorska, W. Maniukiewicz, A. Nosal, J. Ulanski, M. Gazicki-Lipman, *Synth. Met.* **2016**, *220*, 194–201.

[52] T. Yanai, D. P. Tew, N. C. Handy, *Chem. Phys. Lett.* **2004**, *393*, 51–57.

[53] C. Adamo, V. Barone, *J. Chem. Phys.* **1999**, *110*, 6158–6170.

[54] Y. Zhao, D. G. Truhlar, *Theor. Chem. Acc.* **2008**, *120*, 215–241.

[55] M. J. Frisch, G. W. Trucks, H. B. Schlegel, G. E. Scuseria, M. A. Robb, J. R. Cheeseman, G. Scalmani, V. Barone, G. A. Petersson, H. Nakatsuji, X. Li, M. Caricato, A. V. Marenich, J. Bloino, B. G. Janesko, R. Gomperts, B. Mennucci, H. P. Hratchian, J. V. Ortiz, A. F. Izmaylov, J. L. Sonnenberg, D. Williams-Young, F. Ding, F. Lipparini, F. Egidi, J. Goings, B. Peng, A. Petrone, T. Henderson, D. Ranasinghe, V. G. Zakrzewski, J. Gao, N. Rega, G. Zheng, W. Liang, M. Hada, M. Ehara, K. Toyota, R. Fukuda, J. Hasegawa, M. Ishida, T. Nakajima, Y. Honda, O. Kitao, H. Nakai, T. Vreven, K. Throssell, J. A. Montgomery, Jr., J. E. Peralta, F. Ogliaro, M. J. Bearpark, J. J. Heyd, E. N. Brothers, K. N. Kudin, V. N. Staroverov, T. A. Keith, R. Kobayashi, J. Normand, K. Raghavachari, A. P. Rendell, J. C. Burant, S. S. Iyengar, J. Tomasi, M. Cossi, J. M. Millam, M. Klene, C. Adamo, R. Cammi, J. W. Ochterski, R. L. Martin, K. Morokuma, O. Farkas, J. B. Foresman, and D. J. Fox„ Gaussian 16 Revision.A03, **2016**, Gaussian inc., Wallingford, CT.

[56] H. B. Schlegel, *J. Comput. Chem.* **1982**, *3*, 214–218.

[57] N. M. O'Boyle, A. L. Tenderholt, K. M. Langner, *J. Comput. Chem.* **2008**, *29*, 839–845.

[58] F. Bloisi, A. Pezzella, M. Barra, M. Alfè, F. Chiarella, A. Cassinese, L. Vicari, *Appl. Phys. A* **2011**, *105*, 619–627.

[59] M. Barra, D. Viggiano, P. Ambrosino, F. Bloisi, F. V. di Girolamo, M. V. Soldovieri, M. Taglialatela, A. Cassinese, *Biochim. Biophys. Acta Gen. Subj.* **2013**, *1830*, 4365–4373.

[60] F. Chiarella, M. Barra, L. Ricciotti, A. Aloisio, A. Cassinese, *Electronics (Switzerland)* **2014**, *3*, 76–86.